Photoelectrocatalyzed degradation of a pesticides mixture solution (chlorfenvinphos and bromacil) by WO$_3$ nanosheets

G. Roselló-Márquez, R.M. Fernández-Domene, R. Sánchez-Tovar, S. García-Carrión, B. Lucas-Granados, García-Antón, J.

Ingeniería Electroquímica y Corrosión (IEC). Instituto Universitario de Seguridad Industrial, Radiofísica y Medioambiental (ISIRYM). Universitat Politècnica de València.

Camino de Vera s/n, 46022 Valencia, Spain. Tel. 34-96-387 76 32, Fax. 34-96-387 76 39.

E-mail: *jgarciaa@iqn.upv.es* *(J. García-Antón).*

Abstract

A photoelectrocatalyst consisting of WO$_3$ nanosheets or nanorods has been synthesized by electrochemical anodization under hydrodynamic conditions, and has been used for the degradation of two toxic pesticides: chlorfenvinphos and bromacil. Nanostructures have been characterized by FESEM and Raman spectroscopy. Photoelectrochemical degradation tests have been carried out both for individual pesticide solutions and for a mixture solution, and the concentration evolution with time has been followed by UV-Vis spectrophotometry. For individual pesticides, pseudo-first order kinetic coefficients of 0.402 h^{-1} and 0.324 h^{-1} have been obtained for chlorfenvinphos and bromacil, respectively, while for the mixture solution, these kinetic coefficients have been 0.162 h^{-1} and 0.408 h^{-1}. The change in behavior towards pesticide degradation depending on whether individual or mixture solutions were used might be indicative of a competitive process between the two pesticide molecules when interacting with the WO$_3$ nanostructures surface or when approaching the semiconductor/electrolyte interface.

Keywords: photoelectrochemistry; WO$_3$ nanostructures; pesticides; water treatment.

1. Introduction

Pesticides are substances designed to attack plagues principally in the agriculture, but

1

also in the management of public and private green spaces. The exposure to pesticides of organisms that are not their aim, including human beings, can provoke adverse serious effects, diseases and loss of species.

Spain is the European country that uses pesticides the most. In 2014, 78.818 tons of active substances were sold in Spain, which supposed 20 % of all the pesticides sold in Europe that year. This massive use results in a growing presence of pesticide residues in food and in the environment [1].

Pesticides may move from the targeted application sites in several ways. They can be moved through the air, water, attached to soil particles, etc. Pesticide movement away from the application site by wind or air currents is called drift. Pesticides may travel offsite as spray droplets, vapors, dust or solid particles, and even on blowing soil particles. Most pesticides movement in water is either by surface movement off the treated site (runoff) or by downward movement through the soil (leaching). It can occur when too much pesticide is applied or spilled onto a surface or too much rainwater or irrigation water moves pesticide through the soil offsite or into groundwater. Runoff water in an outdoor environment may move into drainage systems, streams, ponds, or other surface water, where the pesticides can travel great distances. And finally, pesticides can also move away from the application site when they are on or in objects or organisms that move offsite, such as the work clothing of pesticide handlers [2, 3].

In this article the degradation of two pesticides used massively worldwide, with high toxicity and persistence, and that have been found in aquifers and wastewaters in various parts of the world [4-8] will be studied. These two pesticides are

chlorfenvinphos and bromacil, whose molecular structures are shown in Figure 1.

Chlorfenvinphos (2-chloro-1-(2,4 dichlorophenyl) vinyl diethyl phosphate) is an organophosphorus insecticide used to control insect pests in livestock. It was also used to control domestic pests such as flies, fleas and mites. This compound has been banned in the European Union (as a phytosanitary product) and in the United States (in 1991) while in Switzerland the use of the Birlane brand is allowed for crops and certain vegetables [9-11]. The toxicity of this compound is due to the inhibition of acetylcholinesterase, causing an accumulation of acetylcholine in the neuroglandular connections and in the Central Nervous System, which generates a hyperexcitation of muscarinic and nicotinic cholinergic receptors, causing different symptoms according to the affected part. It is unknown if this compound is carcinogenic to humans. The Department of Health and Human Environmental Protection Agency has not classified this compound in terms of its carcinogenicity [10-15].

Bromacil (5-bromo-3-sec-butyl-6-methyluracil) is a pesticide that belongs to the family of uracil herbicides. It can be used to selectively control annual and perennial weeds, broadleaf and woody plants on cropland and non-agricultural areas. Bromacil works by interfering with the photosynthetic path of the plants. This herbicide can be sprayed on the plants or spread dry. It dissolves quickly in water and can remain in soil for several years [16-19].

It has been demonstrated that the toxicity of bromacil for invertebrates and fish is in a range between 10 and 100 mg/l while for microalgae this herbicide inhibits its growth at approximate levels of 0.1 mg/L and even lower [15, 20-23]. The toxicity exerted at such

low concentrations would place bromacil in the "extremely toxic" category according to the European Commission's Classification of Contaminants. In addition, it is on the list of priority pollutants of the US Environmental Protection Agency (EPA), which classifies it as a carcinogen for humans [20]

Despite being removed from the EU market, both pesticides are still found in aquifers [5-7, 24, 25]. In addition, there are other countries where their use is allowed, such as Australia [4, 19], Costa Rica [26], South Africa [27], etc.

Therefore, it is interesting to develop strategies to eliminate pesticides from wastewaters due to their harmful effects. Several techniques have been used to that end. Among the most important are the Fenton process and its derivatives [12-14], ozonation [28, 29] and photocatalysis [11, 17, 30-32]. In recent years, photoelectrocatalysis (PEC) has been used to remove persistent organic pollutants due to its interesting advantages [33-35]. Electrolytic and photocatalytic processes are combines in PEC technique, which has the ability to delay the recombination of electron-hole pairs (e^-_{CB} / h^+_{VB}), promoting a greater lifetime of holes. This technique consists of exciting an electron from the valence band (VB) to the conduction band (CB) of a semiconductor, generating a hole in the valence band. To the seminconductor comes radiation with a superior energy to that of the band gap, causing the photoexcitation of the electron from one band to another. The generation of the electron-hole pair occurs by the following reaction:

$$\text{Semiconductor} + h\nu \rightarrow e^-_{CB} + h^+_{VB}$$

(1)
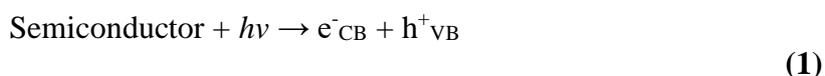
However, the promoted e^-_{CB} is an unstable species and tends to return to its initial state by recombination with unreacted h^+_{VB}, which represents the main inconvenient for the

efficient use of absorbed photons in classical photocatalysis (PC) [33-35].

Therefore, by combining electrochemical and photocatalysis technologies, the recombination of photo-generated electron–hole can be avoided. The applied external potential is a key factor in the PEC technique because it accelerates photocatalytic reaction and hinders recombination [33]. An increase in the efficiency of the PEC is observed, comparing with the classical PC, due to a decrease in the charge recombination generating a greater number of holes. The useful lifetime of photogenerated holes increases and they are more likely to oxidize organic pollutants deposited on the semiconductor surface. In addition, in this technique, the photoanode can be recovered after degradation, using it in successive treatments [33].

In this technique, different oxides can be used as semiconductors, but the most common are TiO_2, Fe_2O_3 and WO_3. In this work, a nanostructure based on WO_3 has been used since this oxide has very good photocatalytic properties. WO_3 is a semiconductor metal oxide, which has the ability to absorb the blue part of the visible spectrum in addition to ultraviolet light. It has a band gap width of approximately 2.6 eV in the monoclinic form. This oxide has a crystal structure formed by octahedrons attached at its corners and its stoichiometry is responsible for many of the properties of the material [36]. The electrical conductivity of WO_3 varies in a range of 10 to 10^{-4} $S \cdot cm^{-1}$ depending on its stoichiometry. On the other hand, as a photocatalytic material, it has the limit of the conduction band (CB) slightly more positive (compared to NHE (normal hydrogen electrode)) than the H_2/H_2O reduction potential and the valence band limit (VB) much more positive than the oxidation potential of H_2O / O_2 (2.803 $V_{Ag/AgCl}$ [37, 38]) which makes WO_3 capable of efficiently producing photo-oxidation in a wide range of organic

compounds. In addition, WO_3 has good stability in acidic environments [36]. However, in spite of all its good properties, nanostructured WO_3 photoanodes have been barely used to degrade persistent organic pollutants, especially if compared with other semiconducting oxides such as TiO_2 [37, 39-46].

The aim of this work is to degrade two highly toxic pesticides with harmful effects for living beings and the environment, chlorfenvinphos and bromacil, by means of PEC using WO_3 nanostructures synthesized by anodization as photoanodes.

2. Materials and methods

2.1. Conditioning of the electrodes (tungsten rods).

Tungsten rods with a diameter of 8 mm and 0.5 cm^2 of cross-sectional area were used as working electrodes. Before anodization, to obtain the desired WO_3 nanostructures, the tungsten electrodes were prepared. The pretreatment consisted of polishing the tungsten bar using different types of sandpaper to obtain a mirror-like surface. Once polished, the surface was washed with distilled water to eliminate any trace of residue from the polishing process and dried with compressed air. Next, the sample was introduced into a small beaker with ethanol to be sonicated for 2 minutes. Finally, the sample was washed again with distilled water and dried with compressed air.

2.2. Electrochemical anodization process.

Once the sample was conditioned, the tungsten rod was subjected to anodization in order to obtain the desired nanostructures. Before anodization, tungsten rods were covered with PTFE except for the surface that was to be anodized (0.5 cm^2). Once covered, the sample was screwed into a rotating electrode, whose rotation speed was set at 375 rpm during anodization. A platinum mesh acted as a cathode. The electrolyte was introduced into an electrochemical cell heated up to 50 ˚C by an external recirculation circuit. The electrolyte composition was 1.5 M H_2SO_4 and 0.05 M H_2O_2. Anodization was performed applying a cell potential of 20 V using a potential source. These experimental conditions were selected according to a previous work [47].

2.3. Post-anodization treatment

The anodized sample was cut and introduced in a cylindrical oven to apply a heat treatment at 400 °C for 4 hours. In this oven the sample was dehydrated and crystalline forms of WO_3 were obtained.

2.4. Nanostructures characterization

The crystalline structure of the samples was characterized by using a Confocal Raman Laser Microscope (neon laser of 632 nm with a power of 420 μW). The composition and crystalline structure of the obtained tungsten oxide nanostructures were analyzed. This characterization of the crystalline structure was carried out before and after the thermal treatment in order to verify if such treatment affected the composition and crystalline structure of the formed nanostructures.

In addition, the surface of the samples was characterized by Field Emission Scanning Electron Microscope (ZEISS ULTRA55 scanning electron microscopy) using 3 kV, to verify the type of nanostructures formed on the substrate.

2.5. Pesticide degradation

Degradation experiments were carried out in a photoelectrochemical quartz reactor. The system was basically composed of a three-electrode electrochemical cell, a potentiostat to provide the external polarization (1V) and a light source to illuminate the photoanode. Irradiations were carried out employing a 1000 W Xe light source and using a visible wavelength of 420 nm. The wavelength was accurately selected by means of a monochromator.

For degradation experiments, 14 mL of the desired solution were put into the reactor with a Ag/AgCl (3M KCl) reference electrode, a Pt counter electrode and the working electrode (WO_3 nanostructures). Before the PEC degradation, this experimental set-up was stirred for 30 min in the dark to allow equilibration of the system. Samples of 2 ml were taken every half hour to monitor the degradation of pesticides through a UV spectrophotometer, recording the absorbance of the solutions on a wavelength range from 190 nm to 500 nm. These samples were then returned to the reactor to continue the degradation.

All tests were performed with a pesticide concentration of 20 ppm and using 0.1 M H_2SO_4 as supporting electrolyte. Degradation of individual pesticides (chlorfenvinphos and bromacil) was carried out, as well as degradation of a mixture of both (20 ppm chlorfenvinphos + 20 ppm bromacil). The duration of these tests was 360 min.

Mineralization of pesticide solutions after 360 min of photoelectrochemical degradation was determined quantifying the decrease in Total Organic Carbon (TOC) by using a Shimadzu TOC-L analyzer.

3. Results and discussion

Figure 2a and Figure 2b show two FESEM images of the WO_3 nanostructure used in this work as photoelectrocatalyst, after the annealing treatment. It can be observed that very thin nanosheets or nanorods were formed on the electrode surface, whose appearance was spongy and very porous (Figure 2a). In the cross-sectional image (Figure 2b), it can be seen that these small nanosheets or nanorods were packed in multiple layers.

Raman spectra of the as-anodized and annealed samples are shown in Figure 2c. Both spectra were similar, although there were some differences. Peaks at 190-195 cm^{-1}, 277 cm^{-1}, 321 cm^{-1}, 713 cm^{-1} and 816 cm^{-1} appeared for both samples and are related to crystalline forms of WO_3 (monoclinic and/or orthorhombic) [48-53]. However, for the as-anodized nanostructure, other peaks can be discerned. These peaks were located between 390-450 cm^{-1} and at 954 cm^{-1}, and are associated respectively with hydrated WO_3 (W–OH_2 bond) [51, 54] and with short terminal W=O bonds [49-52]. These results indicate that partially crystalline WO_3 nanostructures were obtained by anodization, although they needed a thermal treatment to be dehydrated.

As explained above, in this work the degradation of two individual pesticides,

chlorfenvinphos and bromacil, as well as a mixture of both of them, was investigated. Degradation processes were followed by UV-vis spectrophotometry. Figure 3 shows the UV-vis absorption spectra for the two pesticides and for their mixture, at different concentrations. The spectra for chlorfenvinphos (CFV) are presented in Figure 3a. Two well defined peaks can be seen, one at 204 nm and the other at 245 nm. The latter peak has been related to the characteristic chlorfenvinphos aromatic ring $\pi \rightarrow \pi *$ transition and is the peak normally used to follow the degradation of this pesticide [55, 56].

In Figure 3b, UV-vis spectra for different bromacil (BRO) solutions are shown. In this case, three peaks are discerned: a small one at 193 nm and two well-defined and broad peaks at 210 nm and 278 nm. The latter peak can be associated with the uracile group ring. Indeed, it is well known that the UV-vis spectrum for uracil has an absorbance maximum at ~260 nm (in acidic media) [57, 58]. When auxochrome substituents are added to the uracil 5-position (such as the bromine atom in bromacil), the peak associated with the uracil group undergoes a bathochromic shift [57, 58]. Moreover, the peak at ~278 nm has been frequently used to indentify bromacil and to follow its degradation with time [16, 59, 60].

The UV-vis spectra of the mixture solution of chlorfenvinphos and bromacil are presented in Figure 3c. Two broad and more or less defined peaks can be observed at 205 nm and 278 nm, along with a shoulder at short wavelengths (~193 nm) and a band of high absorbance values centered at ~250 nm. In order to assign these features to the different pesticides, the spectra of individual pesticides (at a concentration of 20 ppm) and of the mixture solution (20 ppm CFV + 20 ppm BRO) are shown in Figure 3d. Identifying the different peaks, it is clear that (1) the shoulder at 193 nm observed for

the mixture solution corresponds with the peak at the same wavelength for bromacil; (2) the broad peak centered at 205 nm for the mixture solution is consequence of the peak centered at 204 nm for chlorfenvinphos and the peak centered at 210 nm for bromacil; (3) the flat band with high absorbance values observed for the mixture solution and centered at ~250 nm is a consequence of the chlorfenvinphos peak at 245 nm together with a region of minimum absorbances for bromacil at the same wavelength; (4) the peak at 278 nm for the mixture solution corresponds to the same peak for bromacil.

Therefore, there is correspondence between the absorbance peaks observed for the mixture solution and the peaks of the individual pesticides. Hence, the degradation process of the mixture solution will be followed at the same wavelengths used for individual pesticides, i.e., 245 nm for chlorfenvinphos and 278 nm for bromacil. However, to follow individual degradations from the mixture solution UV-vis spectra, it is necessary to establish the equivalence between the absorbance of individual pesticides and that of the mixture solution, at different concentrations. This equivalence is presented in Figure 4, where each point corresponds to a different concentration (marked in the graphic). It can be observed that absorbance values for chlorfenvinphos in the individual solution, measured at 245 nm, were significantly lower than for the mixture solution, since at this wavelength bromacil also absorbed light (in spite of having a minimum absorbance at this wavelength). On the other hand, absorbance values for individual bromacil were slightly lower than those for the mixture solution, since at 278 nm chlorfenvinphos barely absorbed light and hence almost all absorbance was due to bromacil.

Figure 5a shows the evolution of chlorfenvinphos UV-Vis spectra with

photoelectrochemical degradation time. Absorbance peaks decreased with time, especially that at 245 nm, associated with the aromatic ring (Figure 5a). Since no displacement of this peak was observed during the degradation process, it can be concluded that chlorfenvinphos degradation took place through the aromatic ring opening. After 360 min of irradiation, 91.4 ± 4.6 % of chlorfenvinphos was degraded (Figure 5b). Assuming pseudo-first order kinetics, the kinetic coefficient was determined to be 0.402 ± 0.064 h^{-1} and the mean half-life $t_{1/2} = 1.724$ h.

Figure 6a shows the evolution of bromacil UV-Vis spectra with photoelectrochemical degradation time. It can be observed from Figure 6a that the two peaks at short wavelengths (193 nm and 210 nm) tended to increase with irradiation time and to overlap, forming a single and wide peak centered at ~200 nm. This behavior indicates the formation of intermediate species which absorbed light in that wavelength region. The peak at 278 nm, on the contrary, decreased with irradiation time and did not undergo neither blue nor red shifts. These results suggest that bromacil degradation took place through the cleavage of the uracil ring and the formation of intermediates whose maximum absorbance was at a wavelength of ~200 nm. After 360 min of irradiation, 84.3 ± 3.6 % of bromacil was degraded (Figure 6b). Assuming pseudo-first order kinetics, the kinetic coefficient was determined to be 0.324 ± 0.038 h^{-1} and the mean half-life $t_{1/2} = 2.139$ h, somewhat lower than for chlorfenvinphos.

Figure 7a shows the evolution of the UV-Vis spectra for the mixture solution of 20 ppm chlorfenvinphos and 20 ppm bromacil with photoelectrochemical degradation time. All peaks and absorbance bands decreased with irradiation time, although that decrease was not uniform. The broad peak centered at 205 nm slowly decreased. As it has been

described above, this peak was the consequence of the overlapping of two peaks, one of which decreased with time (204 nm for chlorfenvinphos, see Figure 5a) and the other increased with time (210 nm for bromacil, see Figure 6a). Since the decrease of the chlorfenvinphos peak was more pronounced than the increase of the bromacil peak, the overall result was a small decrease of the combined peak. On the other hand, the absorbance band in the region of intermediate wavelengths also decreased with irradiation time. The absorbance at 245 nm, used to monitor chlorfenvinphos degradation, was therefore significantly smaller after 360 min of irradiation. Finally, the peak at 278 nm, associated with bromacil, also decreased with time, until reaching very low values after 360 min.

According to the UV-Vis spectra shown in Figure 7a for the mixture solution (20 ppm chlorfenvinphos + 20 ppm bromacil) and to the equivalence in absorbances shown in Figure 4, the evolution of the individual pesticides concentration with irradiation time in the mixture solution can be determined. Figure 7b shows the evolution of pesticides concentration with time for the mixture solution and for the individual pesticide solutions (data of individual pesticides has been already presented in Figure 5b and Figure 6b for chlorfenvinphos and bromacil, respectively, but they have been included in Figure 7b for comparison purposes). It can be observed that the temporal evolution of bromacil concentration followed similar tendencies, regardless of the solution treated (individual or mixture solution), and that degradation efficiencies, kinetic coefficients and half-life values after 360 min of irradiation were similar (84.3 % degradation, $k = 0.324$ h^{-1} and $t_{1/2} = 2.139$ h for the individual solution and 90.63% degradation, $k = 0.408$ h^{-1} and $t_{1/2} = 1.699$ h for the mixture solution). The slight increase in bromacil degradation efficiency in the mixture solution can be regarded as not significant since

the differences are approximately within the standard deviation. However, in the case of chlorfenvinphos, photoelectrocatalytic degradation was significantly faster in the case of the individual pesticide (91.4% degradation, $k = 0.402$ h^{-1} and $t_{1/2} = 1.724$ h after 360 min), whereas in the mixture solution, chlorfenvinphos degradation efficiency was only 61.55% after 360 min, the kinetic coefficient was $k = 0.162$ h^{-1} and the half-life was $t_{1/2} = 4.279$ h These results would imply that there was a competition between both pesticides for adsorption sites at the WO$_3$ nanostructures, and that interaction between bromacil and the photoelectrocatalyst surface was favored. At the solution pH (0.1 M H$_2$SO$_4$, pH = ∼ 0.7), the bromacil molecule would be positively charged due to protonation of the amide group, while chlorfenvinphos molecule would be neutral. The different electric charge of pesticide molecules could affect, at least partially, the photoelectrocatalytic degradation mechanism of these pesticides in the mixture solution, and could be a reason for the different behavior in that solution, although future studies will be necessary to confirm that. Another reason of this behavior can be associated with the higher size of the chlorfenvinphos molecule (steric effects); according to the last hypothesis, the approach of the smaller bromacil molecules to the semiconductor/electrolyte solution, where they will react with hydroxyl radicals or directly with photogenerated holes at the WO$_3$ nanostructures surface, would be easier than for chlorfenvinphos molecules.

Finally, in order to quantify the mineralization degree of both pesticides, total organic carbon (TOC) was analyzed. Results are shown in Table 1. It can be observed that the highest mineralization degree was obtained for the chlorfenvinphos solution, while for the bromacil and mixture solutions, TOC decrease was near 50%. These results demonstrate the good properties of WO$_3$ nanosheets/nanorods as visible-light

photoelectrocatalists.

4. Conclusions

The photoelectrochemical degradation of two toxic pesticides, chlorfenvinphos and bromacil, has been carried out using both individual and mixture solutions. It has been shown that in the case of individual solutions, degradation of chlorfenvinphos was slightly favored after 360 min, reaching higher degradation efficiencies than bromacil. However, in the mixture solution, that tendency was the opposite, i.e., bromacil degradation was appreciably faster and its kinetic coefficient was higher than for chlorfenvinphos. This result might be explained by taking into account the possible interactions between the pesticide molecules and the WO_3 nanostructures surface, in which the molecular electric charge (positive in the case of bromacil and neutral in the case of chlorfenvinphos at the solution pH) could play a role, as well as steric effects arising from the different size of pesticide molecules. Further studies would be required to provide an answer to that issue. Nevertheless, the efficiency of WO_3 nanosheets/nanorods as photoelectrocatalysts for the destruction of individual pesticides and mixtures of them has been clearly demonstrated in this work.

References

[1] R. Balaguer, G. Dimastrogiovanni, K. García, E. González, A. Lysimachou, D. Romano. Ríos hormonados: amplia presencia de plaguicidas disruptores endocrinos en los ríos españoles (in Spanish; for the summary in english see: https://www.pan-europe.info/resources/reports/2018/02/r%C3%ADos-hormonados-contamination-spanish-rivers-pesticides#overlay-context=resources/reports; accessed 14 March 2019), Ecologistas en Acción and Pesticide Action Network (PAN) Europe (2018).

[2] L. M. L. Nollet and H. S. Rathore, Handbook of Pesticides: Methods of Pesticide Residues Analysis, CRC Press, Boca Raton, 2009.

[3] K. H. Kim, E. Kabir, S. A. Jahan. Exposure to pesticides and the associated human health effects, Sci. Total Environ. 575 (2017) 525-535.

[4] G. F. Birch, D. S. Drage, K. Thompson, G. Eaglesham, J. F. Mueller. Emerging contaminants (pharmaceuticals, personal care products, a food additive and pesticides) in waters of Sydney estuary, Australia, Mar. Pollut. Bull. 97 (2015) 56-66.

[5] M. Kuzmanovic, A. Ginebreda, M. Petrovic, D. Barceló. Risk assessment based prioritization of 200 organic micropollutants in 4 Iberian rivers, Sci. Total Environ. 503-504 (2015) 289-299.

[6] E. Silva, M. A. Daam, M. J. Cerejeira. Predicting the aquatic risk of realistic pesticide mixtures to species assemblages in Portuguese river basins, J. Environ. Sci. 31 (2015) 12-20.

[7] P. Montuori, S. Aurino, A. Nardone, T. Cirillo, M. Triassi. Spatial distribution and partitioning of organophosphates pesticide in water and sediment from Sarno River and Estuary, Southern Italy, Environ. Sci. Pollut. Res. 22 (2015) 8629-8642.

[8] M. L. Fournier, S. Echeverría-Sáenz, F. Mena, M. Arias-Andrés, E. de la Cruz, C. Ruepert. Risk assessment of agriculture impact on the Frío River watershed and Caño Negro Ramsar wetland, Costa Rica, Environ. Sci. Pollut. Res. 25 (2018) 13347-13359.

[9] H. A. Azab, R. M. Kamel. Binding of chlorfenvinphos and malathion with DNA and their detection using new sensitive luminescent Tb(III) complex probe, J. Lumin. 170 (2016) 671-678.

[10]   J. L. Acero, F. J. Real, F. Javier Benitez, A. González. Oxidation of chlorfenvinphos in ultrapure and natural waters by ozonation and photochemical processes, Water Res. 42 (2008) 3198-3206.

[11]   M. I. Maldonado, P. C. Passarinho, I. Oller, W. Gernjak, P. Fernández, J. Blanco, S. Malato. Photocatalytic degradation of EU priority substances: A comparison between TiO_2 and Fenton plus photo-Fenton in a solar pilot plant, J. Photochem. Photobiol. A: Chem. 185 (2007) 354-363.

[12]   M. I. Maldonado Rubio, W. Gernjak, I. Oller Alberola, J. Blanco Gálvez, P. Fernández-Ibáñez, S. Malato Rodríguez. Photo-Fenton degradation of alachlor, atrazine, chlorfenvinphos, diuron, isoproturon and pentachlorophenol at solar pilot plant, Int. J. Environ. Pollut. 27 (2006) 125-146.

[13]   C. Oliveira, A. Alves, L. M. Madeira. Treatment of water networks (waters and deposits) contaminated with chlorfenvinphos by oxidation with Fenton's reagent, Chem. Eng. J. 241 (2014) 190-199.

[14]   N. Klamerth, W. Gernjak, S. Malato, A. Agüera, B. Lendl. Photo-Fenton decomposition of chlorfenvinphos: Determination of reaction pathway, Water Res. 43 (2009) 441-449.

[15]   S. S. Liu, X. Q. Song, H. L. Liu, Y. H. Zhang, J. Zhang. Combined photobacterium toxicity of herbicide mixtures containing one insecticide, Chemosphere 75 (2009) 381-388.

[16]   J. V. Sancho, C. Hidalgo, F. Hernández. Direct determination of bromacil and diuron residues in environmental water samples by coupled-column liquid chromatography and large-volume injection, J. Chromatogr. A 761 (1997) 322-326.

[17]   H. K. Singh, M. Muneer, D. Bahnemann. Photocatalysed degradation of a herbicide derivative, bromacil, in aqueous suspensions of titanium dioxide, Photochem. Photobiol. Sci. 2 (2003) 151-156.

[18]   M. Ibáñez, J. V. Sancho, O. J. Pozo, F. Hernández. Use of quadrupole time-of-flight mass spectrometry to determine proposed structures of transformation products of the herbicide bromacil after water chlorination, Rapid Commun. Mass Spectrom. 25 (2011) 3103-3113.

[19]   A. M. Davis, P. J. Thorburn, S. E. Lewis, Z. T. Bainbridge, S. J. Attard, R. Milla, J. E. Brodie. Environmental impacts of irrigated sugarcane production: Herbicide run-off dynamics from farms and associated drainage systems, Agr. Ecosyst. Environ. 180 (2013) 123-135.

[20]   U.S.Environmental Protection Agency (EPA). Reregistration Elegibility Decision (RED) for Bromacil (https://archive.epa.gov/pesticides/reregistration/web/pdf/0041red.pdf; accessed 14 March 2019).   1996.

[21] C. R. Seery, L. Gunthorpe, P. J. Ralph. Herbicide impact on Hormosira banksii gametes measured by fluorescence and germination bioassays, Environ. Pollut. 140 (2006) 43-51.

[22] P. C. Wilson, S. B. Wilson. Toxicity of the herbicides bromacil and simazine to the aquatic macrophyte, *Vallisneria americana* Michx, Environ. Toxicol. Chem. 29 (2009) 201-211.

[23] M. Brycht, T. Özmen, B. Burnat, K. Kaczmarska, A. Leniart, M. Tastekin, E. Kiliç, S. Skrzypek. Voltammetric behavior, quantitative determination, and corrosion investigation of herbicide bromacil, J. Electroanal. Chem. 770 (2016) 6-13.

[24] V. Belenguer, F. Martinez-Capel, A. Masiá, Y. Picó. Patterns of presence and concentration of pesticides in fish and waters of the Júcar River (Eastern Spain), J. Hazard. Mater. 265 (2014) 271-279.

[25] B. Szatkowska, M. Kwiatkowska, J. Michalowicz, P. Sicinska, B. Huras, B. Bukowska. Impact of chlorfenvinphos, an organophosphate insecticide on human blood mononuclear cells (in vitro), Pestic. Biochem. Phys. 102 (2012) 175-181.

[26] S. Echeverría-Sáenz, F. Mena, M. Pinnock, C. Ruepert, K. Solano, E. de la Cruz, B. Campos, J. Sánchez-Avila, S. Lacorte, C. Barata. Environmental hazards of pesticides from pineapple crop production in the Río Jiménez watershed (Caribbean Coast, Costa Rica), Sci. Total Environ. 440 (2012) 106-114.

[27] J. M. Dabrowski, J. M. Shadung, V. Wepener. Prioritizing agricultural pesticides used in South Africa based on their environmental mobility and potential human health effects, Environ. Int. 62 (2014) 31-40.

[28] M. I. Maldonado, S. Malato, L. A. Pérez-Estrada, W. Gernjak, I. Oller, X. Doménech, J. Peral. Partial degradation of five pesticides and an industrial pollutant by ozonation in a pilot-plant scale reactor, J. Hazard. Mater. 138 (2006) 363-369.

[29] K. Ikehata, M. Gamal El-Din. Aqueous Pesticide Degradation by Ozonation and Ozone-Based Advanced Oxidation Processes: A Review (Part II), Ozone Sci. Eng. 27 (2005) 173-202.

[30] L. Muszkat, L. Feigelson, L. Bir, K. A. Muszkat. Photocatalytic degradation of pesticides and bio-molecules in water, Pest Manag. Sci. 58 (2002) 1143-1148.

[31] B. Paul, W. N. Martens, R. L. Frost. Immobilised anatase on clay mineral particles as a photocatalyst for herbicides degradation, Appl. Clay Sci. 57 (2012) 49-54.

[32] D. Angthararuk, P. Sutthivaiyakit, C. Blaise, F. Gagné, S. Sutthivaiyakit. Photo-catalysis of bromacil under simulated solar light using Au/TiO$_2$: evaluation of main degradation products and toxicity implications, Environ. Sci. Pollut. Res. 22 (2015) 1468-1479.

[33] R. Daghrir, P. Drogui, D. Robert. Photoelectrocatalytic technologies for environmental applications, J. Photoch. Photobio. A 238 (2012) 41-52.

[34] S. Garcia-Segura, E. Brillas. Applied photoelectrocatalysis on the degradation of organic pollutants in wastewaters, J. Photoch. Photobio. C 31 (2017) 1-35.

[35] M. G. Peleyeju, O. A. Arotiba. Recent trend in visible-light photoelectrocatalytic systems for degradation of organic contaminants in water/wastewater, Environ. Sci.: Water Res. Technol. 4 (2018) 1389-1411.

[36] H. Zheng, J. Z. Ou, M. S. Strano, R. B. Kaner, A. Mitchell, K. Kalantar-zadeh. Nanostructured Tungsten Oxide - Properties, Synthesis, and Applications, Adv. Funct. Mater. 21 (2011) 2175-2196.

[37] R. M. Fernández-Domene, R. Sánchez-Tovar, B. Lucas-Granados, M. J. Muñoz-Portero, J. García-Antón. Elimination of pesticide atrazine by photoelectrocatalysis using a photoanode based on WO_3 nanosheets, Chem. Eng. J. 350 (2018) 1114-1124.

[38] L. Weinhardt, M. Blum, M. Bär, C. Heske, B. Cole, B. Marsen, E. L. Miller. Electronic Surface Level Positions of WO_3 Thin Films for Photoelectrochemical Hydrogen Production, J. Phys. Chem. C 112 (2008) 3078-3082.

[39] S.S. Thind, M. Tian, A. Chen. Direct growth and photo-electrochemical study of WO_3 nanostructured materials, Electrochem. Commun. 43 (2014) 13–17.

[40] Q. Zheng, C. Lee. Visible light photoelectrocatalytic degradation of methyl orange using anodized nanoporous WO_3, Electrochim. Acta 115 (2014) 140-145.

[41] S.S. Thind, K. Rozic, F. Amano, A. Chen. Fabrication and photoelectrochemical study of WO3-based bifunctional electrodes for environmental applications, Appl. Catal. B Environ. 176-177 (2015) 464-471.

[42] S. Xie, K. Ouyang. Degradation of refractory organic compounds by photocatalytic fuel cell with solar responsive WO_3/FTO photoanode and air-breathing cathode, J. Colloid Interface Sci. 500 (2017) 220–227.

[43] J. Zheng, J. Li, J. Bai, X. Tan, Q. Zeng, L. Li, B. Zhou. Efficient degradation of refractory organics using sulfate radicals generated directly from WO_3 photoelectrode and the catalytic reaction of sulfate, Catalysts 7 (2017) 346.

[44] R.M. Fernández-Domene, R. Sánchez-Tovar, B. Lucas-Granados, C.S. García-Zamora, J. García-Antón. Customized WO_3 nanoplatelets as visible-light photoelectrocatalyst for the degradation of a recalcitrant model organic compound (methyl orange), J. Photochem. Photobiol. A Chem. 356 (2018) 46–56.

[45]   R.M. Fernández-Domene, R. Sánchez-Tovar, B. Lucas-Granados, M.J. Muñoz-Portero, R. Ramírez-Grau, J. García-Antón. Visible-light photoelectrodegradation of diuron on WO_3 nanostructures, J. Environ. Manage. 226 (2018) 249-255.

[46]   R.M. Fernández-Domene, G. Roselló-Márquez, R. Sánchez-Tovar, B. Lucas-Granados, J. García-Antón. Photoelectrochemical removal of chlorfenvinphos by using WO_3 nanorods: Influence of annealing temperature and operation pH, Sep. Purif. Technol. 212 (2019) 458-464.

[47]   R. M. Fernández-Domene, R. Sánchez-Tovar, B. Lucas-Granados, G. Roselló-Márquez, J. García-Antón. A simple method to fabricate high-performance nanostructured WO_3 photocatalysts with adjusted morphology in the presence of complexing agents, Mater. Design 116 (2017) 160-170.

[48]   B. Pecquenard, H. Lecacheux, J. Livage, C. Julien. Orthorhombic WO_3 Formed via a Ti-Stabilized $WO_3 \cdot 13H_2O$ Phase, J. Solid State Chem. 135 (1998) 159-168.

[49]   A. G. Souza-Filho, V. N. Freire, J. M. Sasaki, J. Mendes Filho, J. F. Julião, U. U. Gomes. Coexistence of triclinic and monoclinic phases in WO_3 ceramics, J. Raman Spectrosc. 31 (2000) 451-454.

[50]   C. Bittencourt, R. Landers, E. Llobet, X. Correig, J. Calderer. The role of oxygen partial pressure and annealing temperature on the formation of W = O bonds in thin WO_3 films, Semicond. Sci. Technol. 17 (2002) 522-525.

[51]   A. Z. Sadek, H. Zheng, M. Breedon, V. Bansal, S. K. Bhargava, K. Latham, J. Zhu, L. Yu, Z. Hu, P. G. Spizzirri, W. Wlodarski, K. Kalantar-zadeh. High-Temperature Anodized WO_3 Nanoplatelet Films for Photosensitive Devices, Langmuir 25 (2009) 9545-9551.

[52]   F. Amano, M. Tian, B. Ohtani, A. Chen. Photoelectrochemical properties of tungsten trioxide thin film electrodes prepared from facet-controlled rectangular platelets, J. Solid State Electrochem. 16 (2012) 1965-1973.

[53]   H. Song, Y. Li, Z. Lou, M. Xiao, L. Hu, Z. Ye, L. Zhu. Synthesis of Fe-doped WO_3 nanostructures with high visible-light-driven photocatalytic activities, Appl. Catal. B-Environ. 166-167 (2015) 112-120.

[54]   M. F. Daniel, B. Desbat, J. C. Lassegues, B. Gerand, M. Figlarz. Infrared and Raman study of WO_3 tungsten trioxides and WO_3, xH_2O tungsten trioxide tydrates, J. Solid State Chem. 67 (1987) 235-247.

[55]   A. Bojanowska-Czajka, A. Galezowska, J. L. Marty, M. Trojanowicz. Decomposition of pesticide chlorfenvinphos in aqueous solutions by gamma-irradiation, J. Radioanal. Nucl. Chem. 285 (2010) 215-221.

[56] T. Sharifi, Y. Ghayeb, T. Mohammadi. Study of conformational changes in serum albumin by binding of chlorfenvinphos using multispectroscopic techniques and molecular dynamic simulation, Monatsh. Chem. 148 (2017) 781-791.

[57] M. M. Stimson. The Ultraviolet Absorption Spectra of Some Pyrimidines. Chemical Structure and the Effect of pH on the Position of λ_{max}, J. Am. Chem. Soc. 71 (1949) 1470-1474.

[58] T. Gustavsson, N. Sarkar, Á. Bányász, D. Markovitsi, R. Improta. Solvent Effects on the Steady-state Absorption and Fluorescence Spectra of Uracil, Thymine and 5-Fluorouracil, Photochem. Photobiol. 83 (2007) 595-599.

[59] E. Ayranci, N. Hoda. Studies on removal of metribuzin, bromacil, 2,4-d and atrazine from water by adsorption on high area carbon cloth, J. Hazard. Mater. 112 (2004) 163-168.

[60] T. Polubesova, S. Nir, D. Zadaka, O. Rabinovitz, C. Serban, L. Groisman, B. Rubin. Water Purification from Organic Pollutants by Optimized Micelle-Clay Systems, Environ. Sci. Technol. 39 (2005) 2343-2348.

Table caption

Table 1. Initial and final total organic carbon (TOC) values, as well as mineralization degree (in %) for the individual pesticide solutions and for the mixture solution.

Figure Captions

Figure 1. a) Chlorfenvinphos molecular structure; b) Bromacil molecular structure

Figure 2. a) FESEM top image of the WO_3 nanostructure; b) FESEM cross-sectional image of the WO_3 nanostructure; c) Raman spectra of the as-anodized and annealed WO_3 nanostructure.

Figure 3. a) UV-Vis spectra for different chlorfenvinphos (CFV) solutions; b) UV-Vis spectra for different bromacil (BRO) solutions; c) UV-Vis spectra for different mixture (MIX: CFV + BRO) solutions; d) UV-Vis spectra for the individual pesticide solutions (20 ppm) and the mixture solution (20 ppm + 20 ppm).

Figure 4. Absorbance equivalence between individual pesticide solutions and mixture solution.

Figure 5. a) Evolution of chlorfenvinphos UV-Vis spectra with photoelectrochemical

degradation time; b) variation of the quotient between the chlorfenvinphos concentration at a given time (C) and the initial concentration (C_0) with photoelectrochemical degradation time.

Figure 6. a) Evolution of bromacil UV-Vis spectra with photoelectrochemical degradation time; b) variation of the quotient between the bromacil concentration at a given time (C) and the initial concentration (C_0) with photoelectrochemical degradation time.

Figure 7. a) Evolution of the mixture solution UV-Vis spectra with photoelectrochemical degradation time (initial concentrations of 20 ppm chlorfenvinphos + 20 ppm bromacil); b) variation of the quotient between the pesticide concentration at a given time (C) and the initial concentration (C_0) with photoelectrochemical degradation time, for individual chlorfenvinphos (CFV) and bromacil (BRO), and for these pesticides in the mixture solution.

Figure 1.

(a)

(b)

Figure 2

(a)

(b)

As-anodized

Annealed
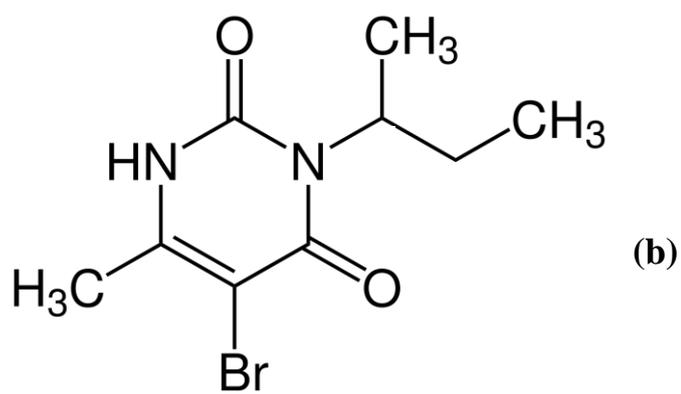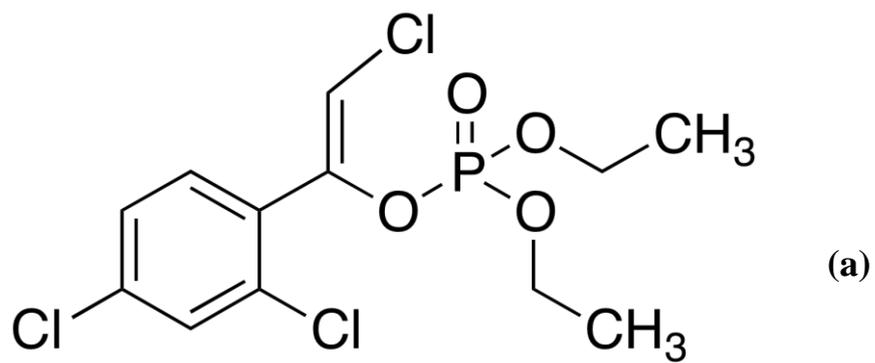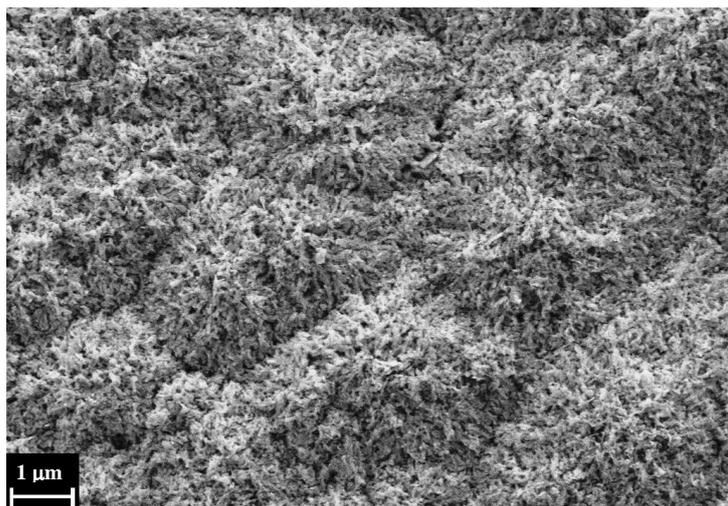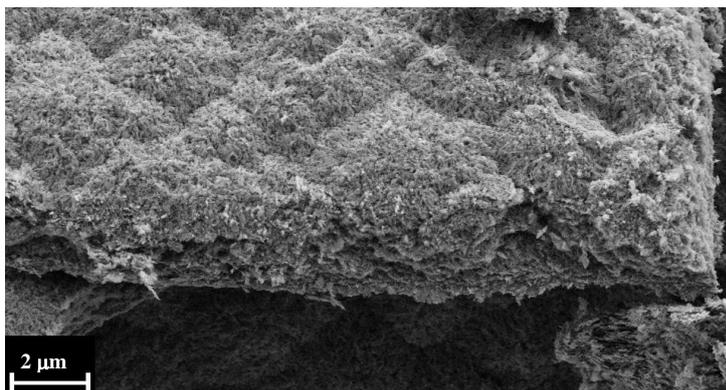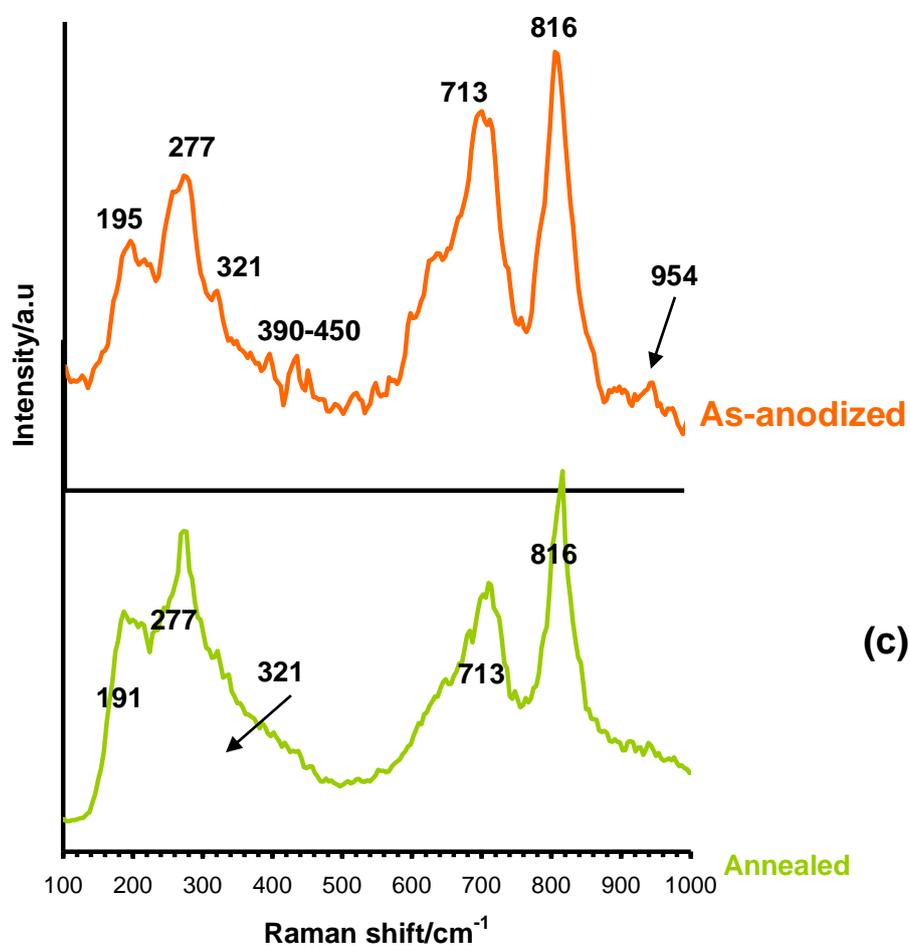
(c)
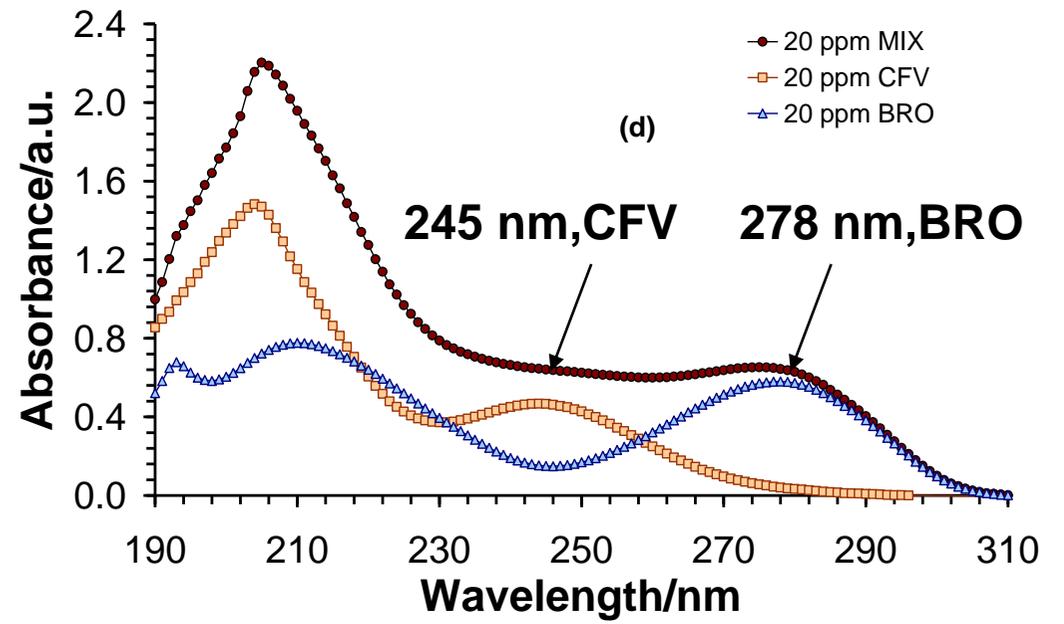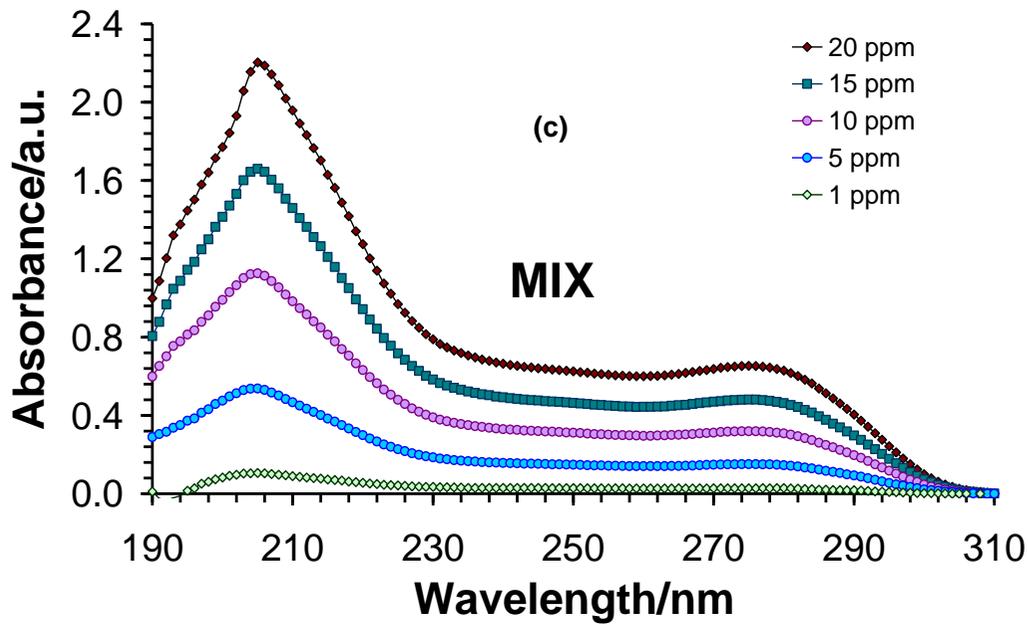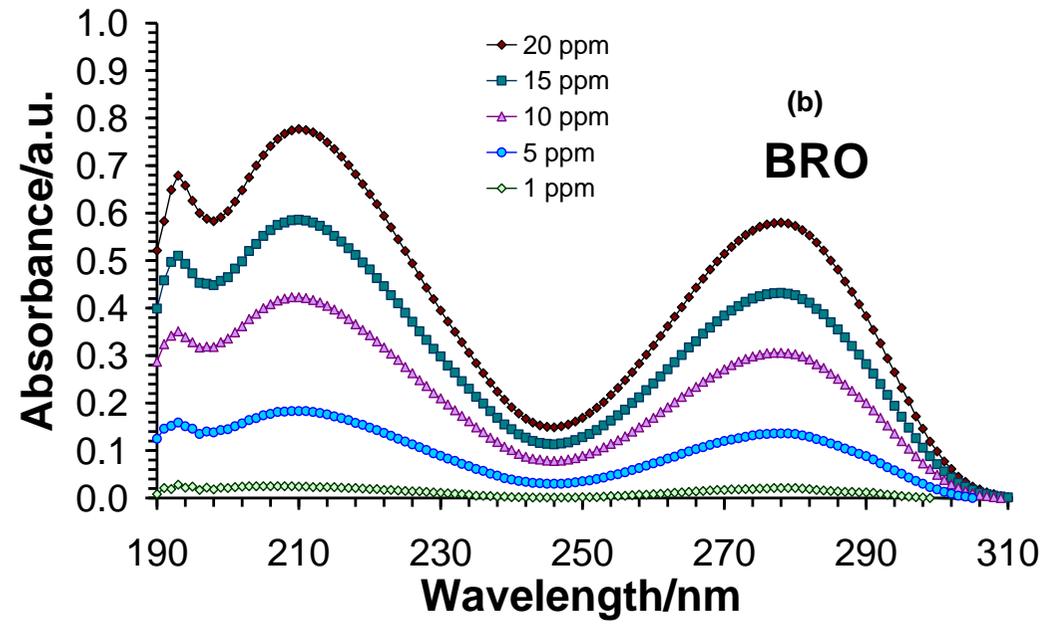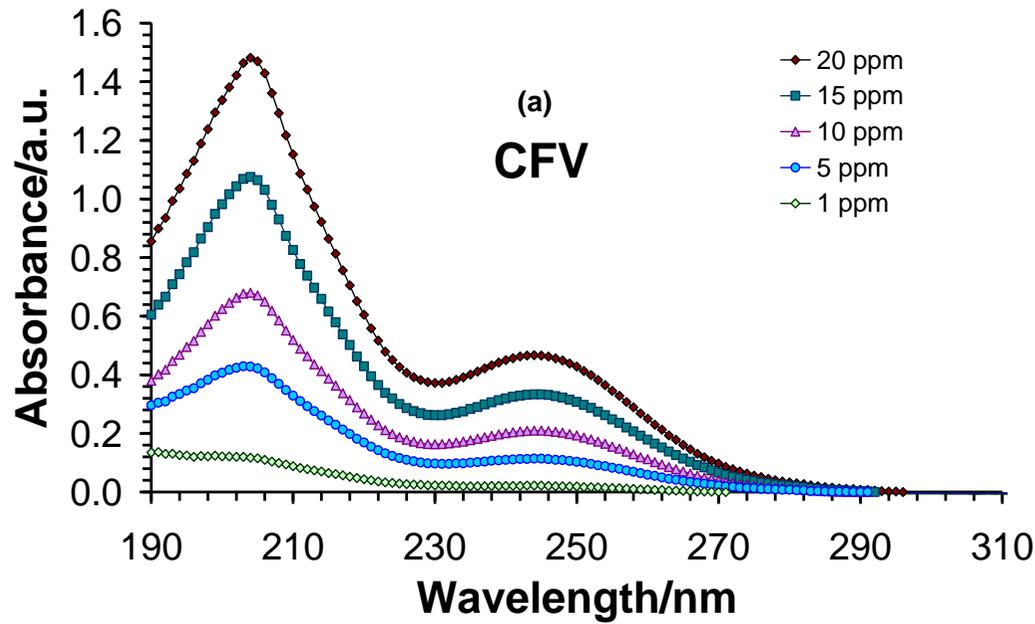
Figure 3

1   **Figure 4**

2

3
4
5
6
7
8
9
10
11
12
13
14
15
16
17
18
19
20

Figure 5

(b)
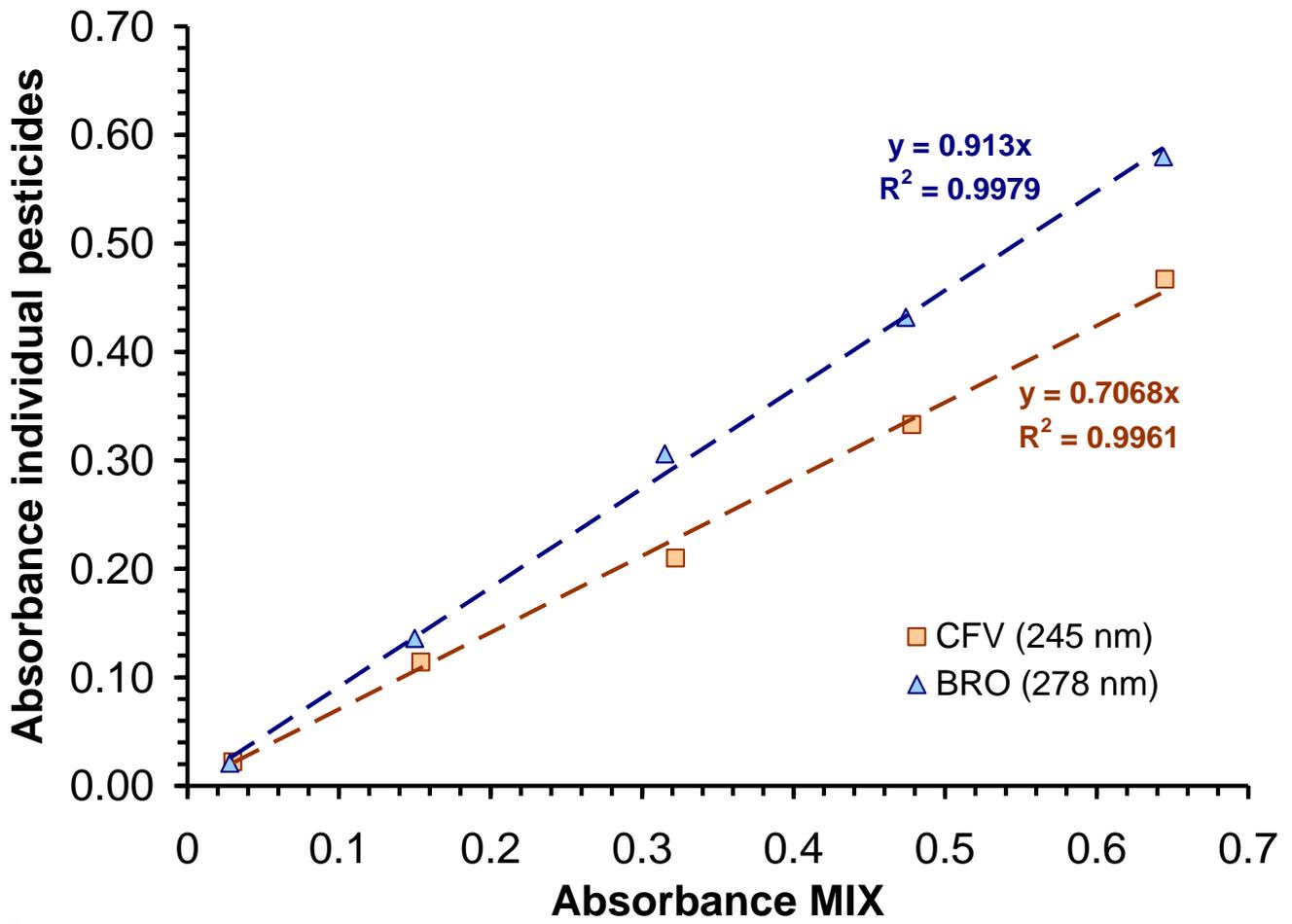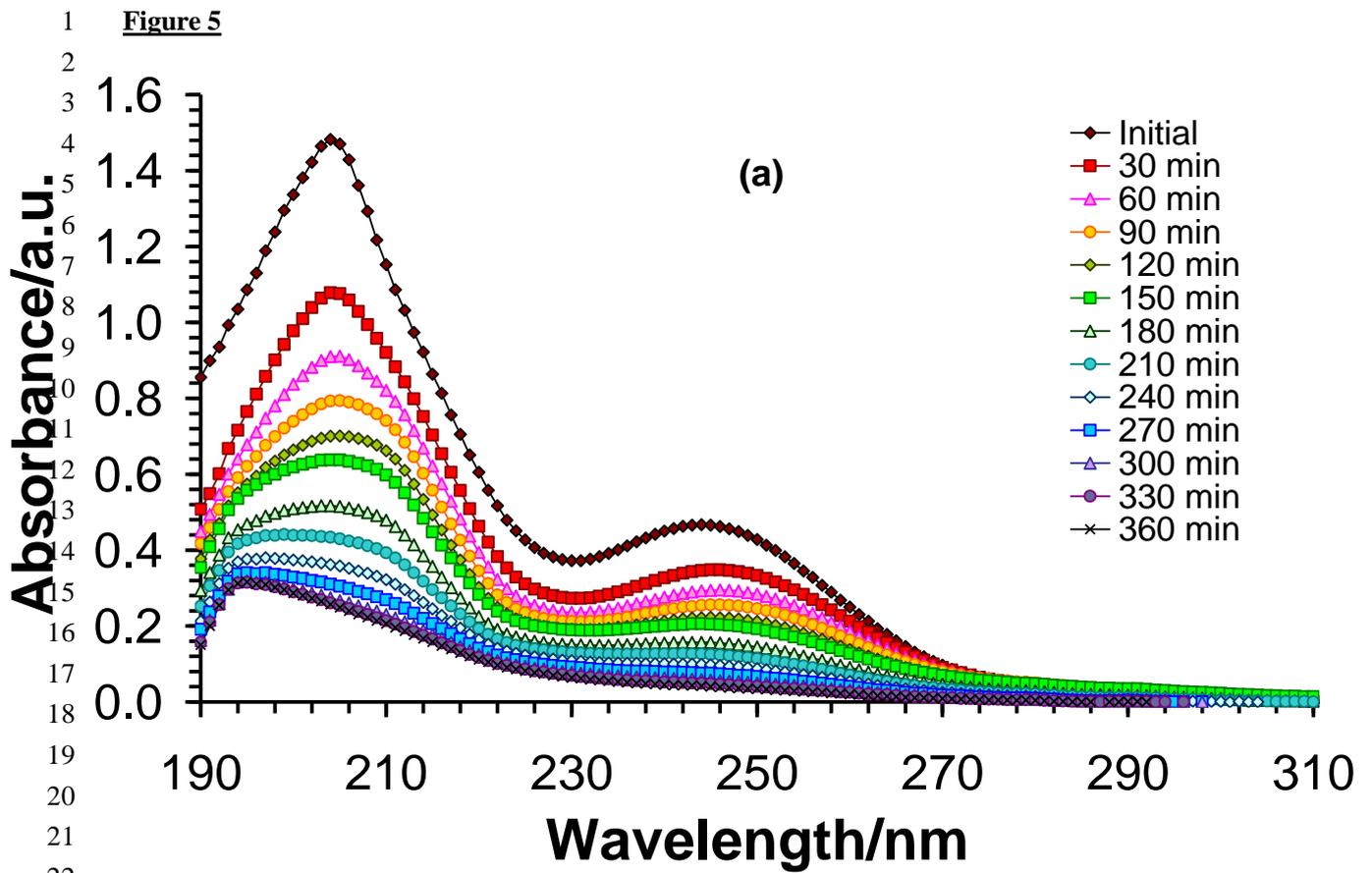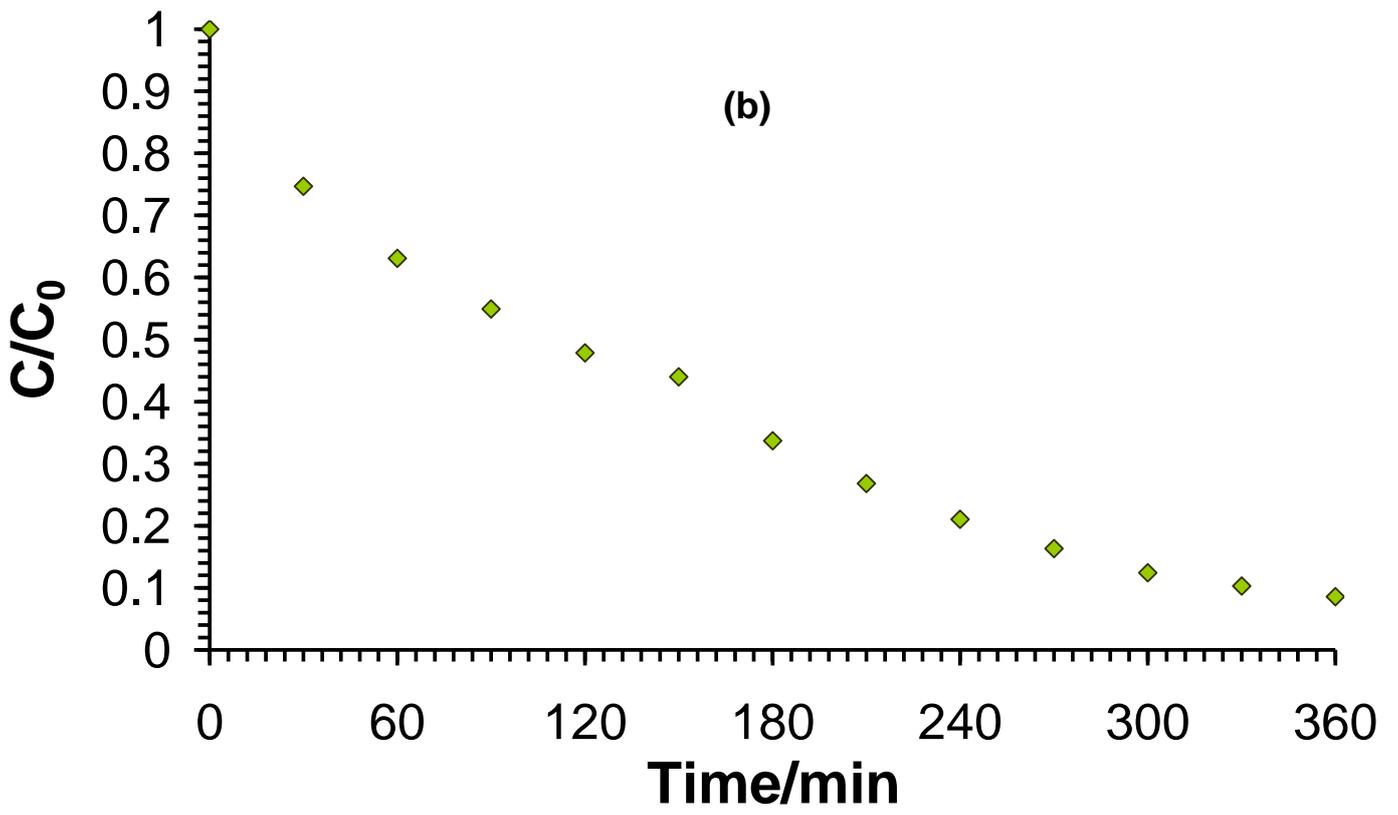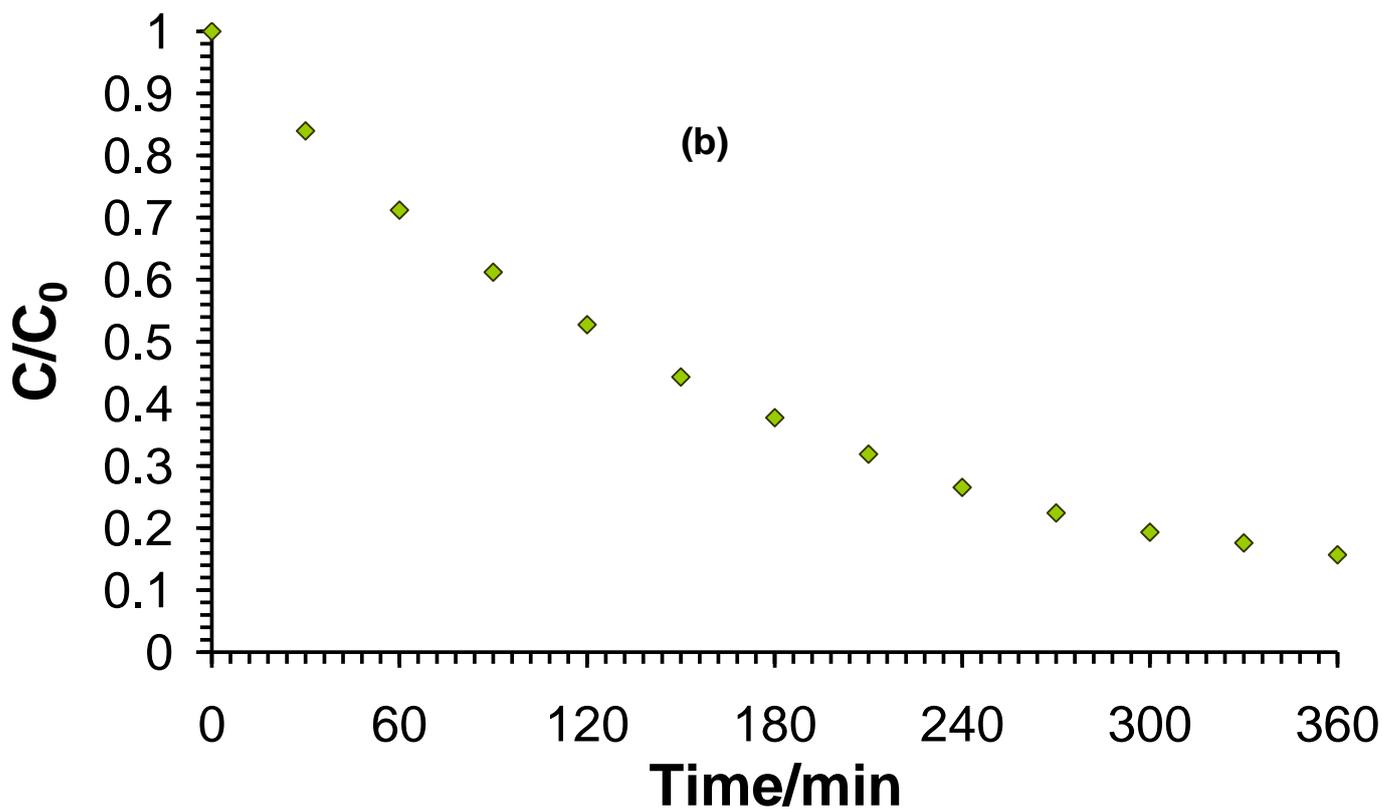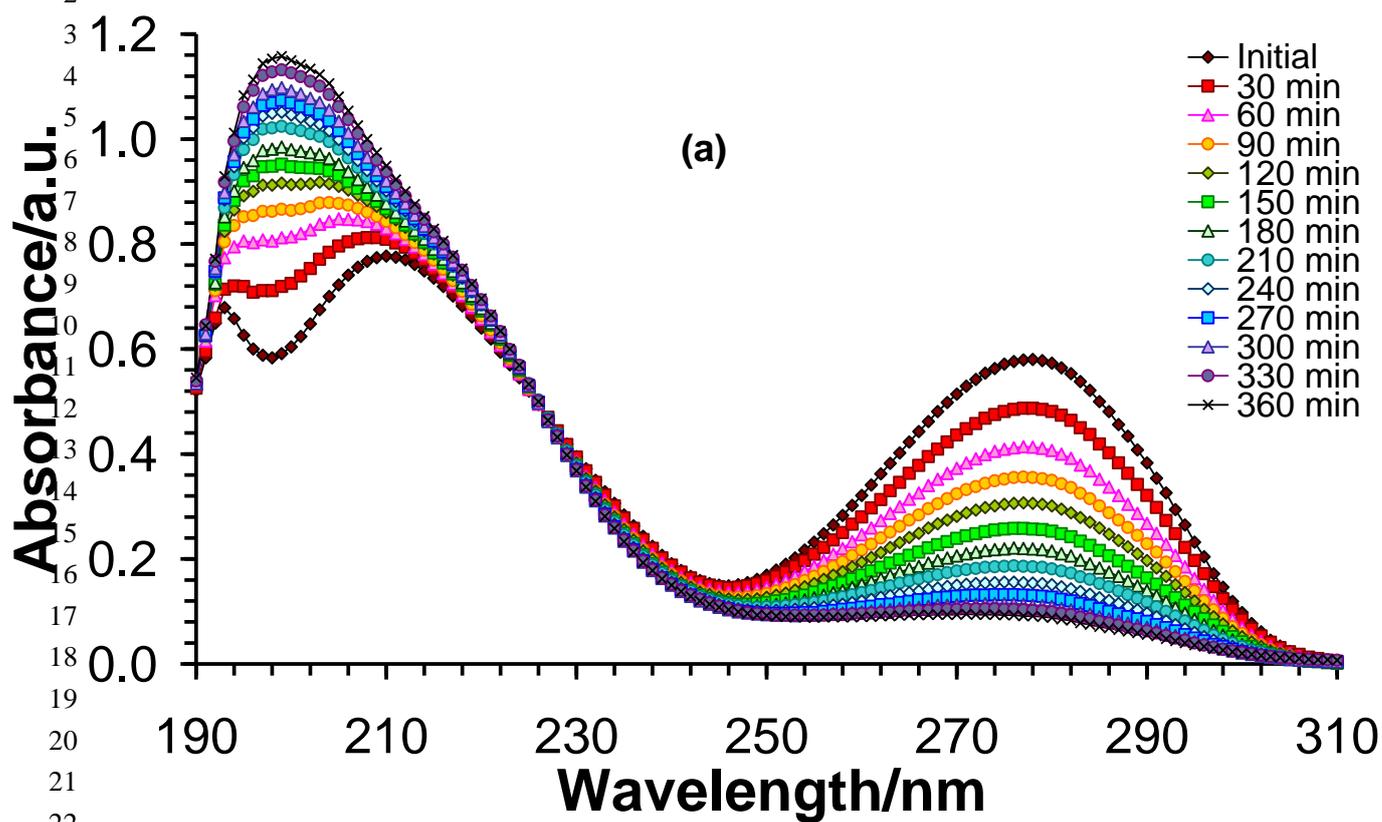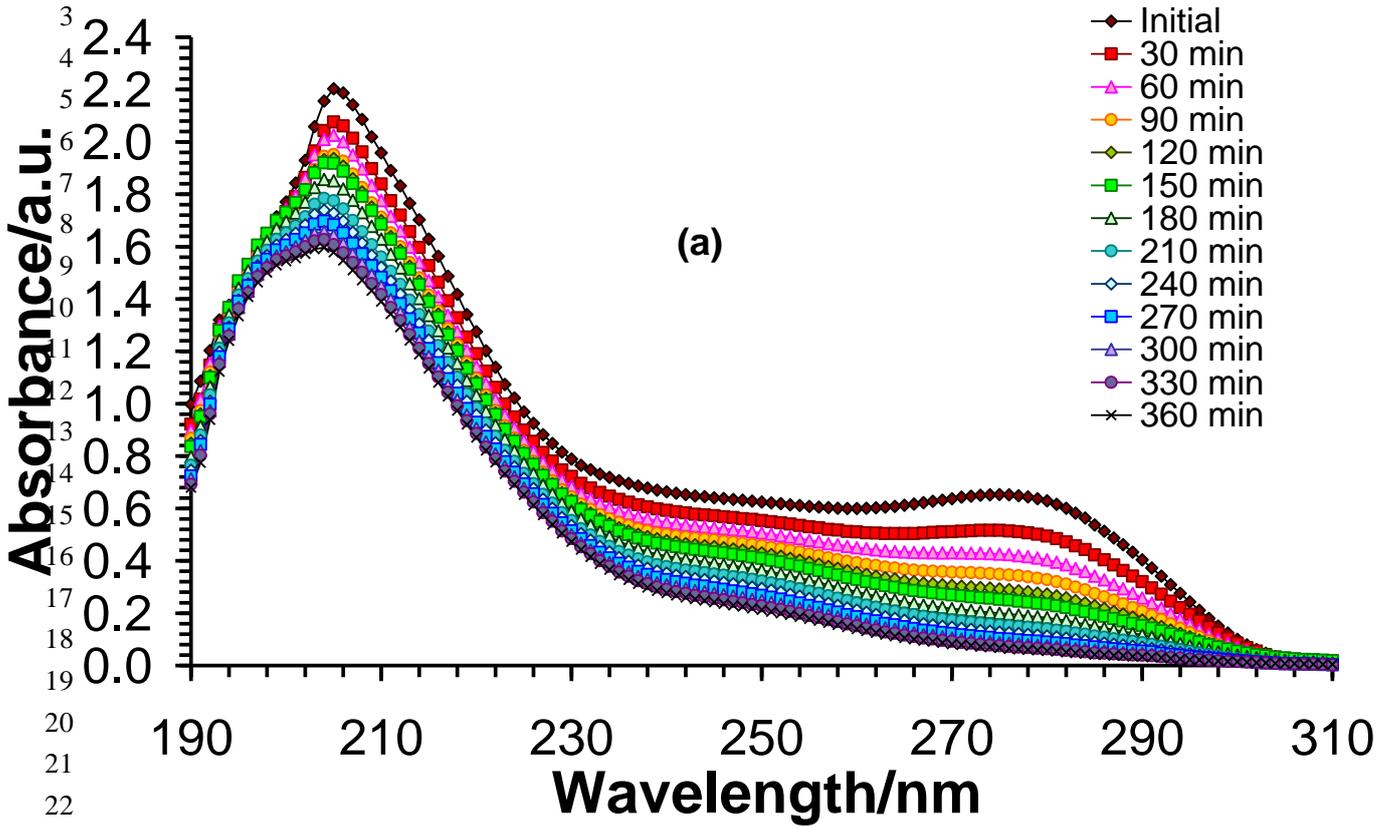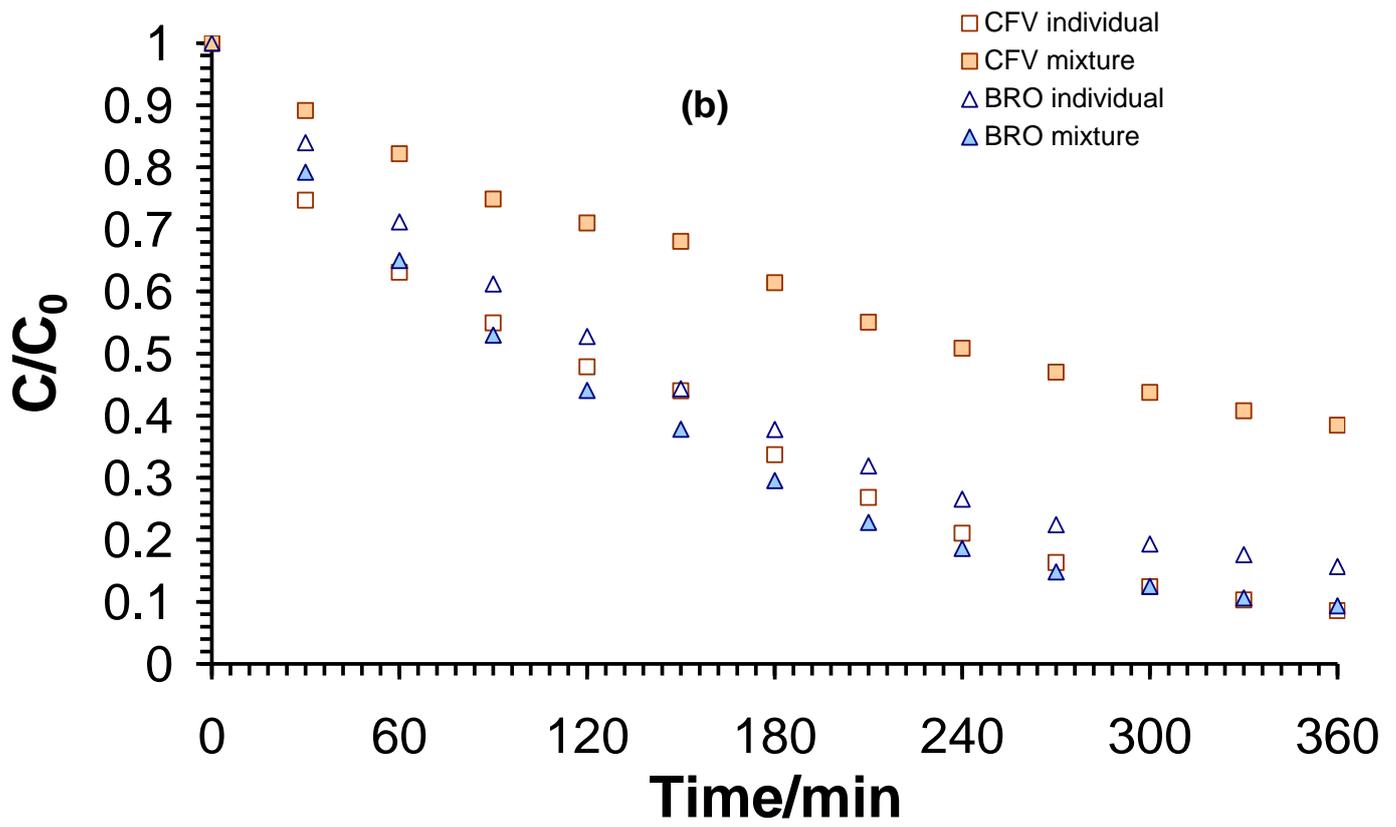
1
2
3
4
5
6
7
8
9
10
11
12
13
14
15
16
17
18
19
20
21
22
23

Figure 6

1

2

3   **Table 1**

4

5

Solution	Initial TOC/ppm	Final TOC/ppm	% mineralization
CFV (individual)	8.02	3.16	60.53
BRO (individual)	8.33	4.76	42.86
Mixture	16.25	8.55	47.39

6

7

8

9

10